Electronic Supplementary Material (ESI) for Physical Chemistry Chemical Physics.

XAS investigation of silica aerogel supported cobalt rhenium catalysts for ammonia decomposition.

Karsten G. Kirste[a], Said Laassiri[b], Zhigang Hu[c], Dragos Stoian[d], Laura Torrente-Murciano[c*], Justin S.J. Hargreaves[e*], Karina Mathisen[a*]

[a]*Department of Chemistry, Norwegian University of Science and Technology, Høgskoleringen 5, N-7491 Trondheim, Norway*
[b]*Chemical & Biochemical Sciences. Green Process Engineering (CBS). Mohamed VI Polytechnic University, UM6P, 43150, Ben Guerir, Morocco*
[c]*Department of Chemical Engineering and Biotechnology, University of Cambridge, CB3 0AS, Cambridge, UK*
[d]*Swiss-Norwegian Beamline, European Synchrotron Radiation Facility, F-38043, Grenoble cedex, France*
[e]*School of Chemistry, Joseph Black Building, University of Glasgow, Glasgow G12 8QQ, UK*

Authors to whom correspondence should be addressed:lt416@cam.ac.uk; karina.mathisen@ntnu.no; Justin.Hargreaves@glasgow.ac.uk

Supplementary Information:

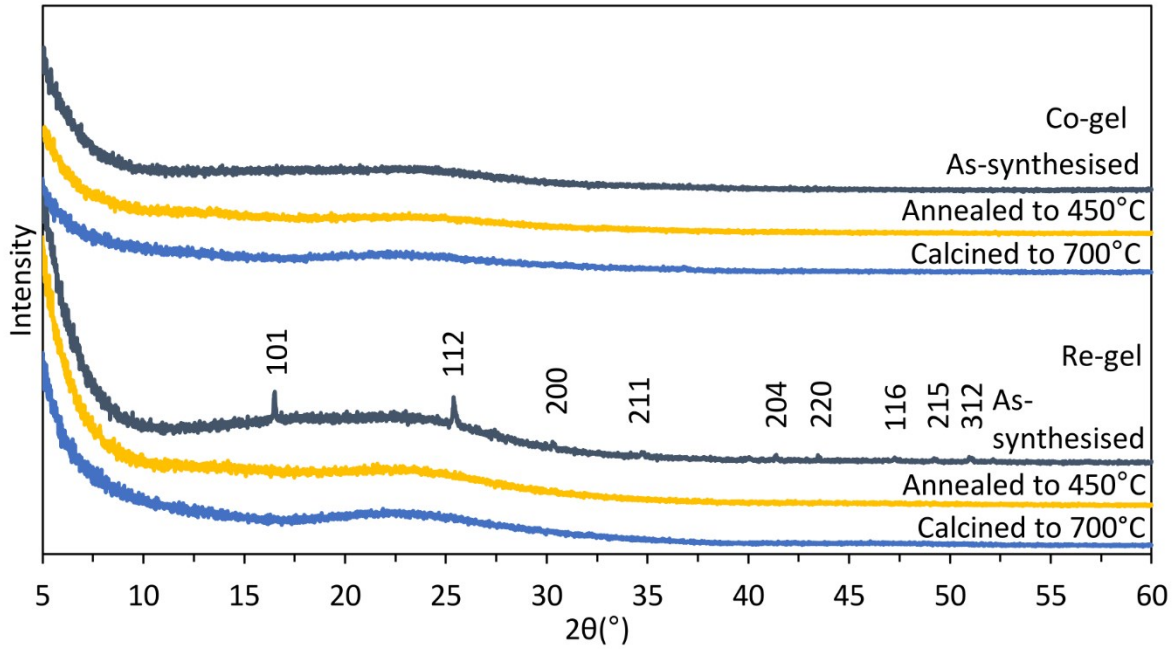

S 1. XRD of the as synthesised, annealed and calcined Co-gel and Re-gel, where the reflections of the as-synthesised Re-gel match NH_4ReO_4 (PDF 000-010-0252, ICDD, 2020).

Table S 1. Metal loading and surface area for the different thermally treated monometallic gels.

Material	Thermal treatment	Co (wt.%) [a]	Re (wt.%) [a]	Surface Area ($m^2\ g^{-1}$) [b]	$<P_d>$ (nm) [c]	V_c ($cm^3\ g^{-1}$) [d]
CoRe-gel	As-synthesised	3.0	2.7	595	3.5	0.76
	Annealed			758	3.6	0.74
	Calcined			566	3.6	0.54
Co-gel	As-synthesised	2.9	-	688	4.1	0.94
	Annealed	2.9	-	833	4.2	1.05
	Calcined	3.3	-	635	4.2	0.73
Re-gel	As-synthesised	-	1	588	3.5	0.88
	Annealed	-	0.2	742	3.4	0.86
	Calcined	-	0.1	802	3.6	0.78
Plain-gel	As-synthesised	-	-	614	2.7	0.34
	Annealed	-	-	847	2.5	0.33
	Calcined	-	-	680	2.3	0.15

[a] RSD is estimated to ± 0.07 p.p

[b] Calculated from BET method from N_2 adsorption

[c] Calculated from the BJH method based in N_2 desorption isotherm

[d] Calculated from the BJH method at the relative pressure p p_0^{-1} = 0.98

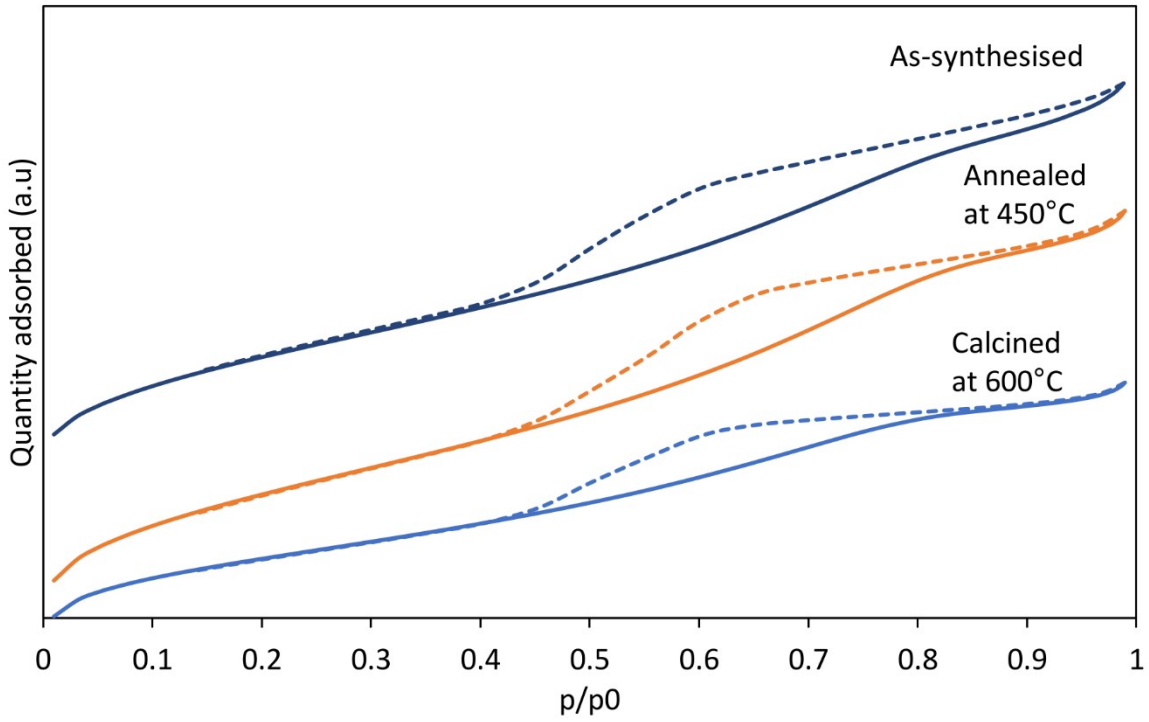

S 2.The stacked nitrogen adsorption isotherms of the as synthesised, annealed and calcined Co-gels.

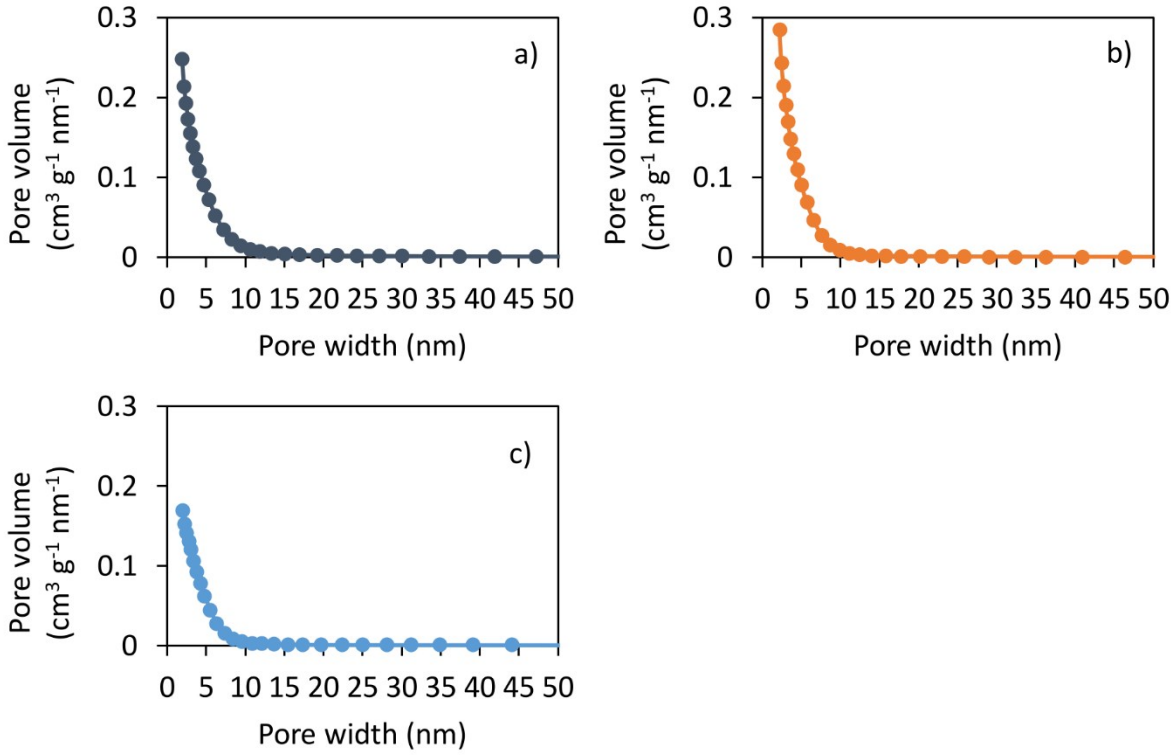

S 3. The pore size distributions of a) as-synthesised, b) annealed, c) calcined CoRe-aerogel.

Table S 2. Results of Fourier filtered of the second shell in the annealed CoRe-gel at the Co K-edge (Real space range is 2.3-3 Å, the chi curves are fitted in the k-range of 3-10 $Å^{-1}$ with AFAC=0.66)

Shell	N	R (Å)	$2\sigma^2$ ($Å^2$)	E_F (eV)	R (%)
Co…Co	3.2(6)	2.90(1)	0.043(5)	3(1)	37
Co…O	1.6(2)	2.897(8)	0.011(3)	-4.5(5)	37
Co…Re	3.6(5)	2.999(9)	0.033(3)	3.4(6)	40
Co…Si	2.2(1)	3.098(3)	0.020(1)	6.2(3)	12

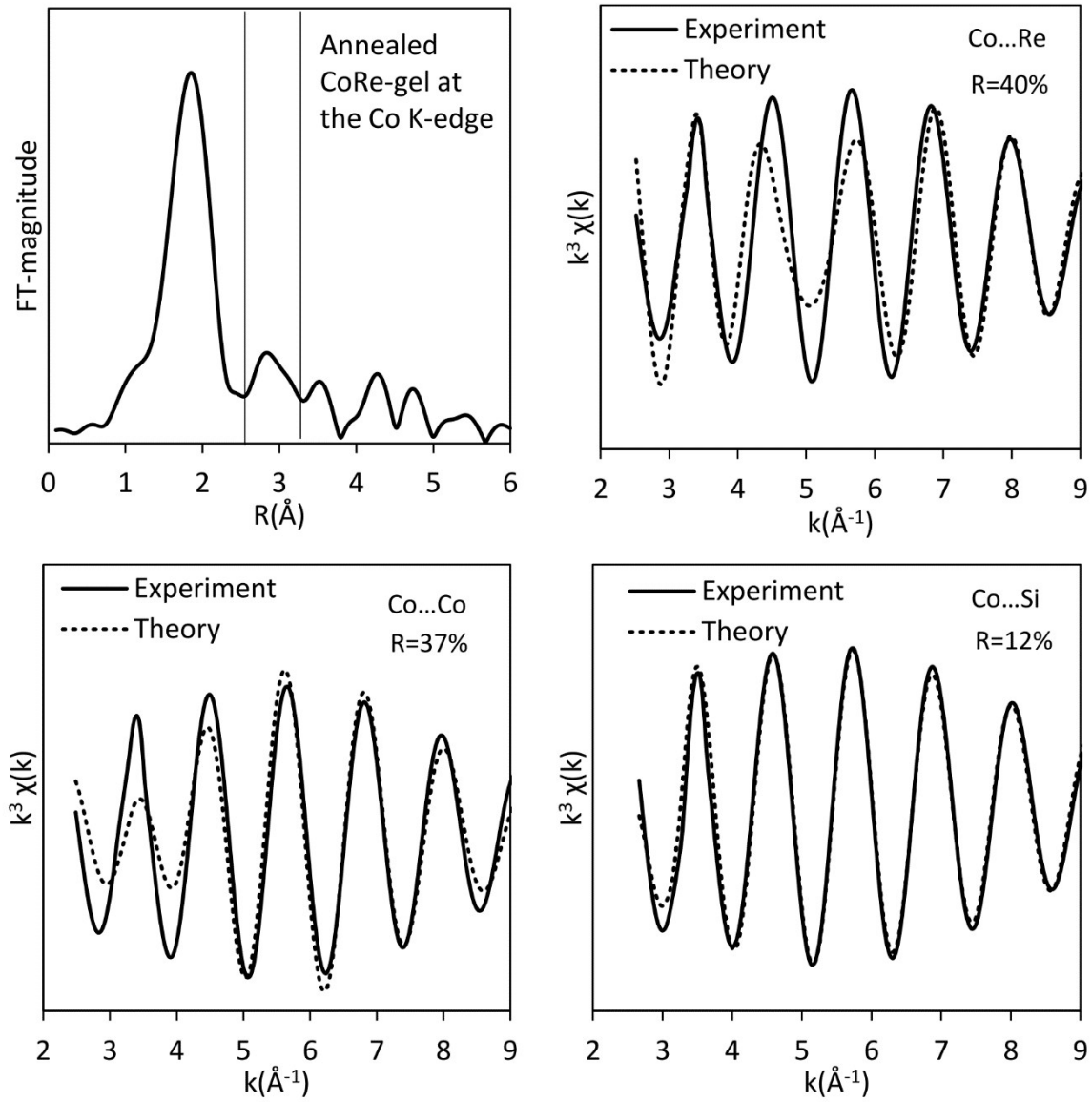

S 4. Fourier filtered and fitted backscattered signal originating (Real space range: 2.3-3.0 Å) from the second shell in the annealed CoRe-gel at the Co K-edge.

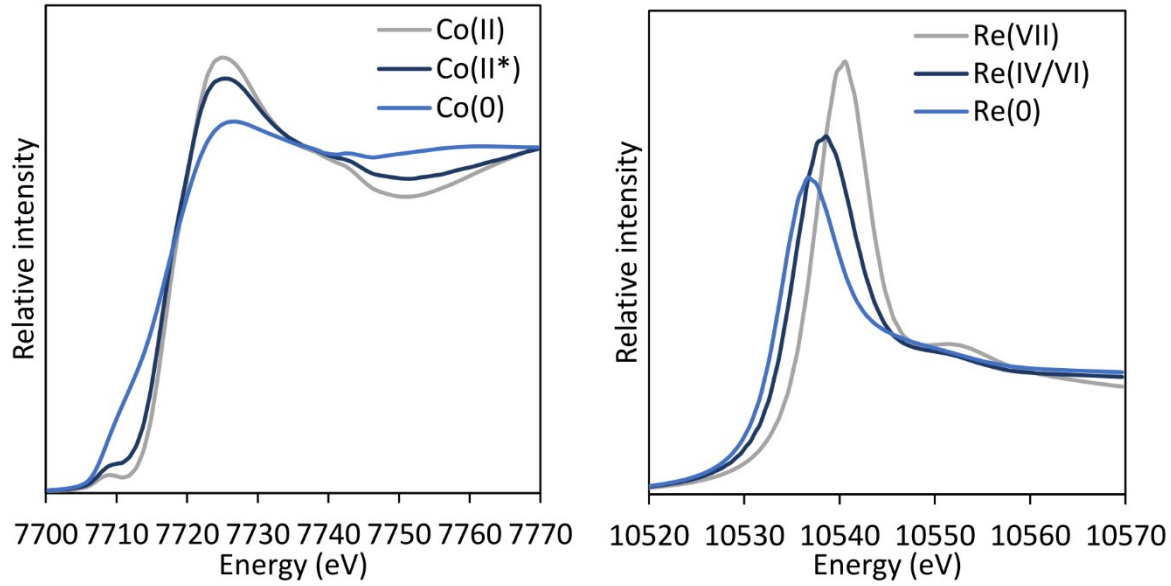

S 5. Cobalt components (left) and rhenium components (right) in the MCR-analysis of the CoRe-gel during the pre-treatment in 75% H_2 during the pre-treatment.

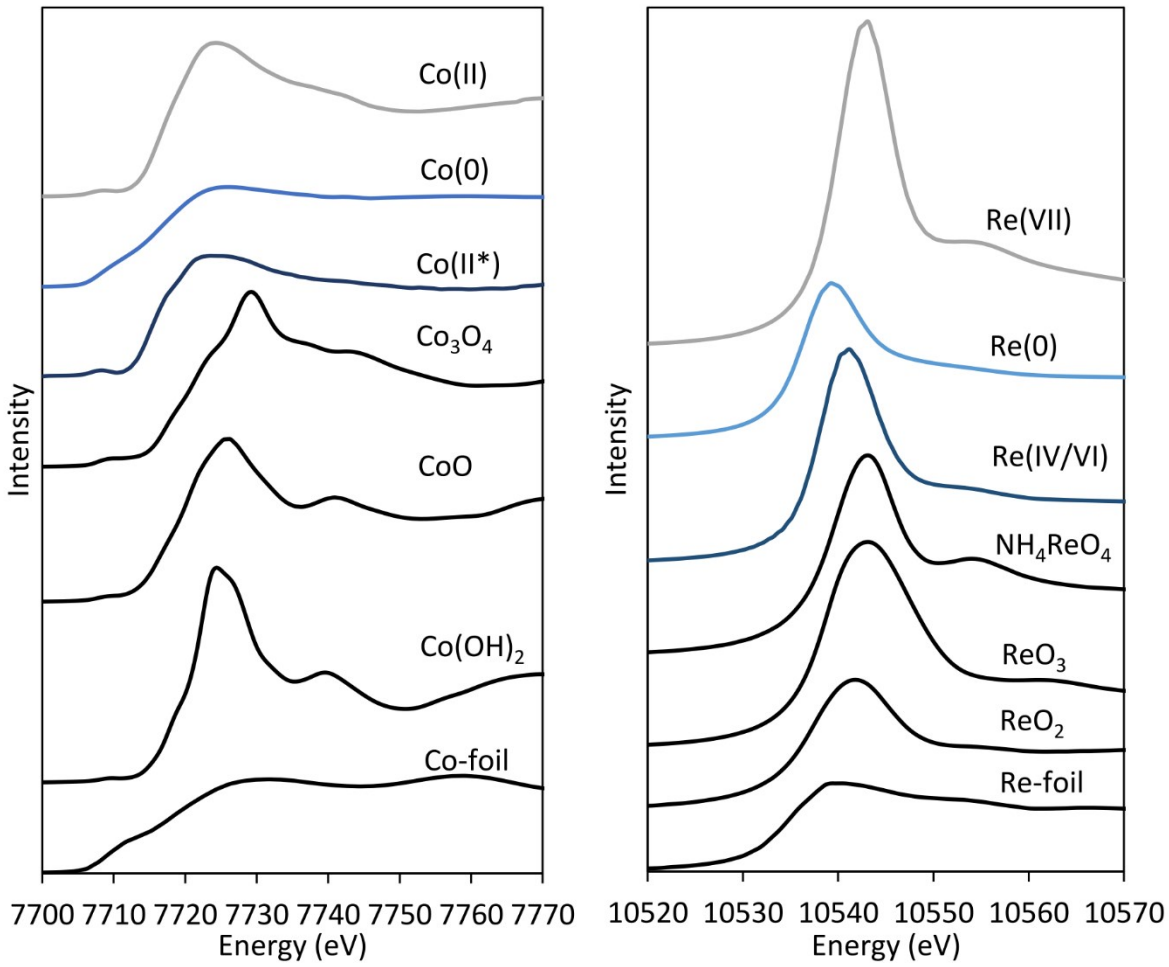

S 6. MCR-analysis components compared with references at the Co K-edge (left) and Re L_{III}-edge (right).

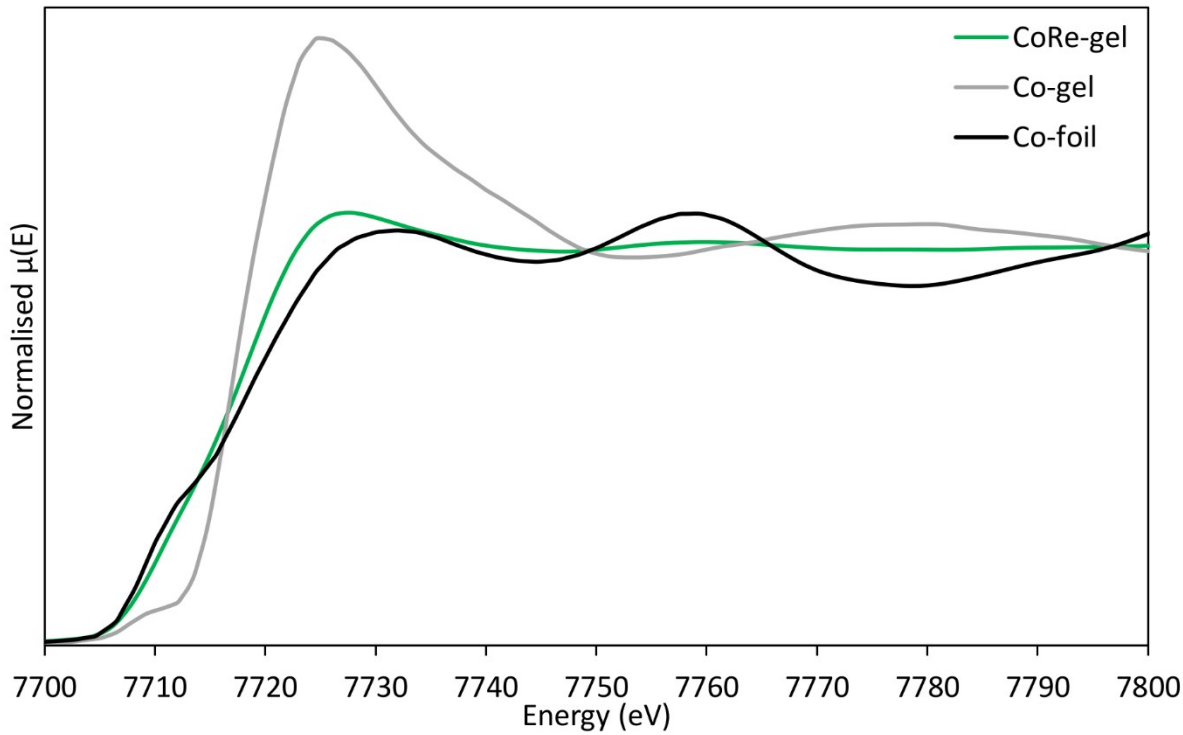

S 7. Normalised XANES after pre-treatment in 75% H_2 at the cobalt K-edge.

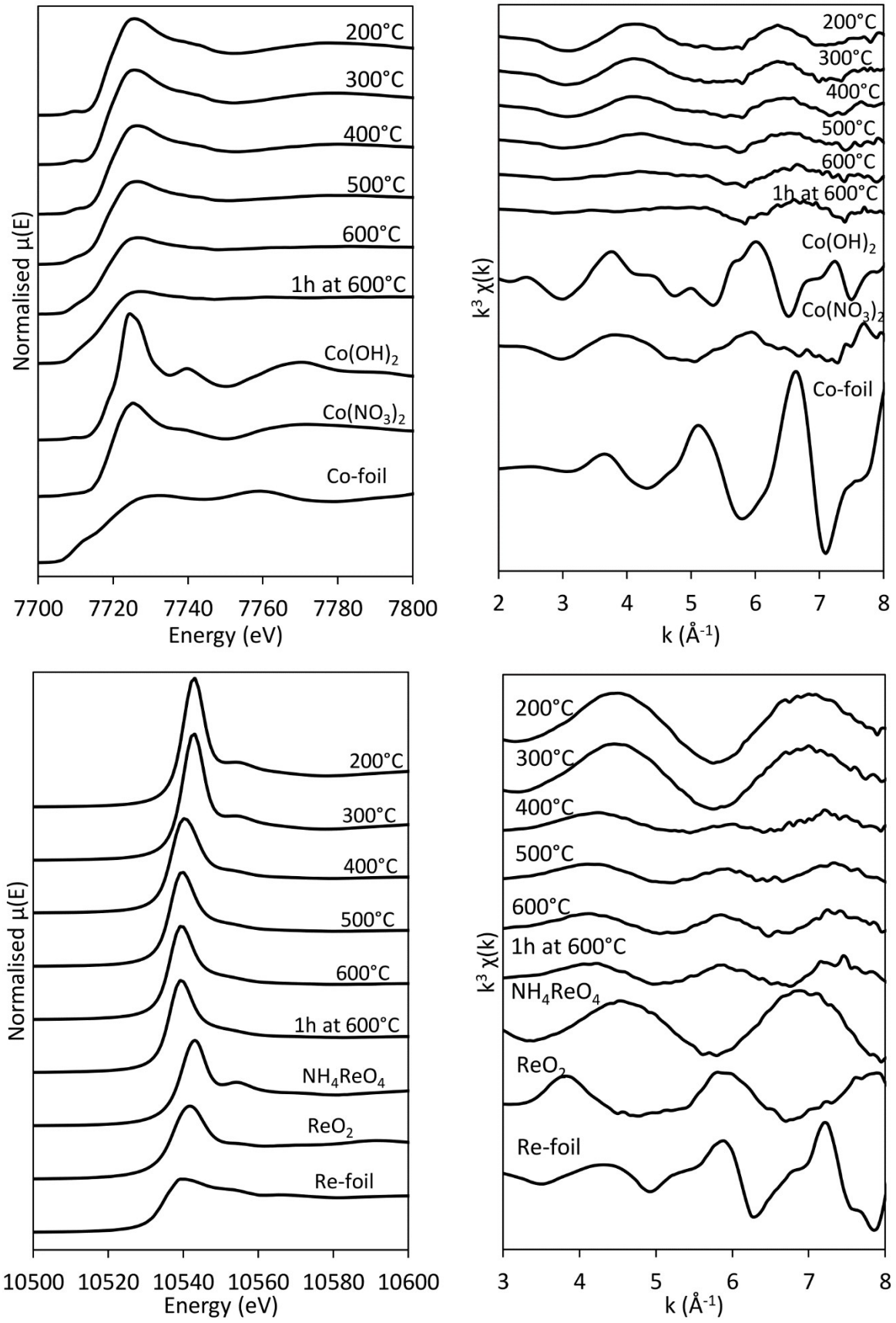

S 8. XANES of the reduction of the CoRe-gel from the Co K-edge (top) and the Re L_{III}-edge (bottom) during pre-treatment with absorption edges (left) and chi curves (right).

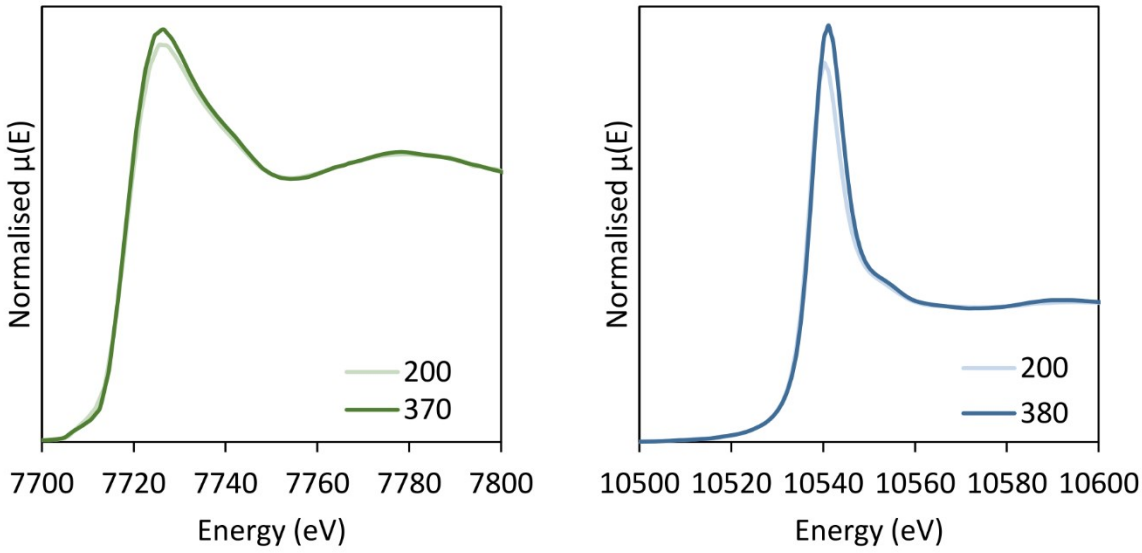

S 9. XANES of the CoRe-gel at the Co K-edge (left) and Re L_{III}-edge (right) at 200°C and 370/380°C in 5% NH_3.

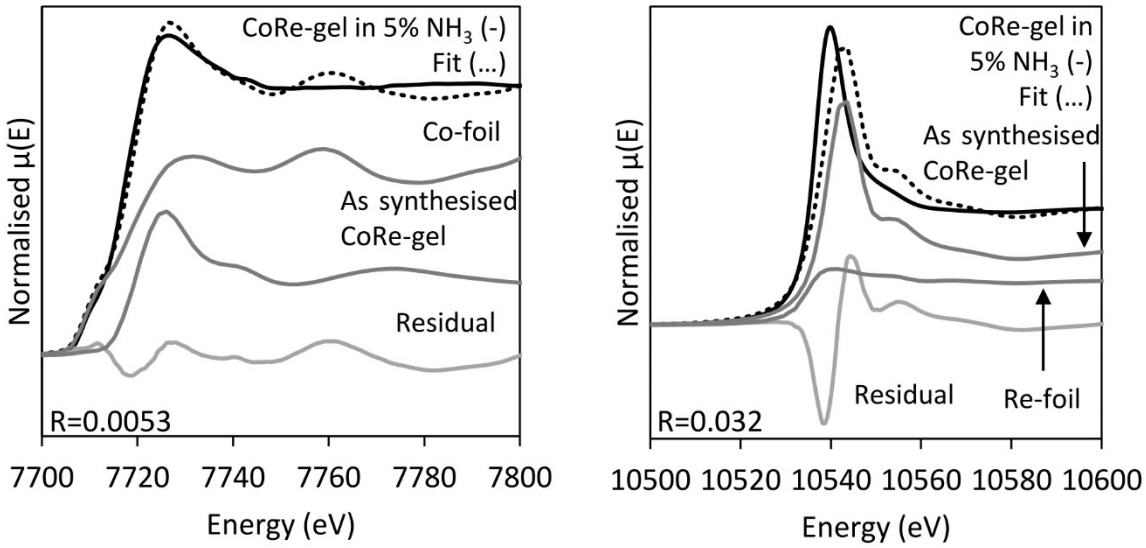

S 10. Linear combinations of the CoRe-gel in 5% NH_3 at 600°C with the as synthesised material and Co-foil (left) at the Co K-edge and the Re-foil (right) at the Re L_{III}-edge.

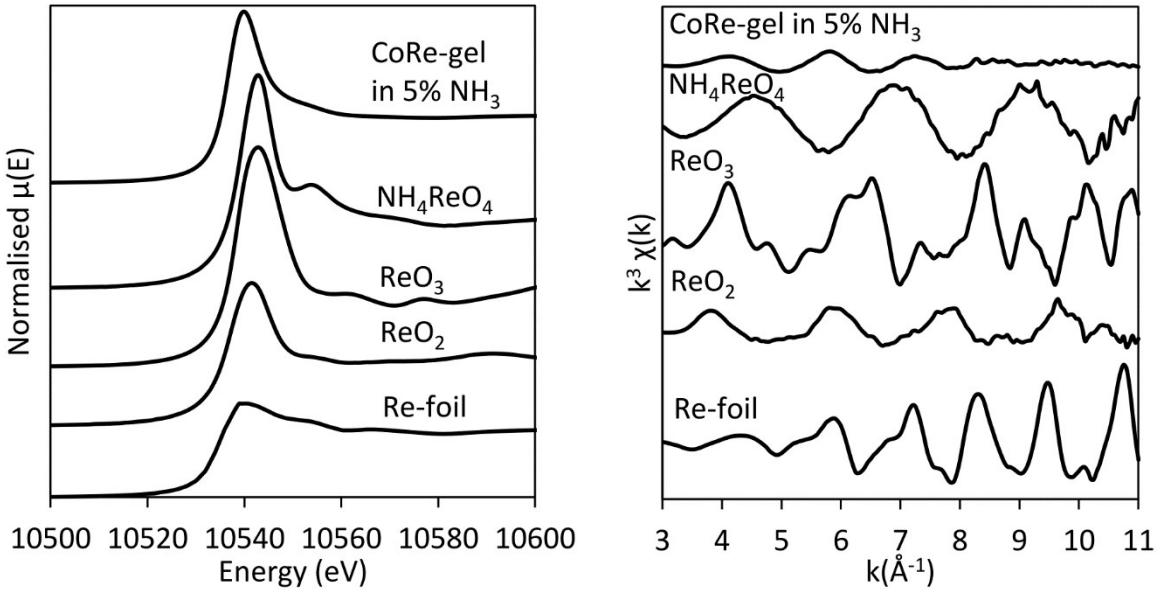

S 11. The XANES (left) and the chi curves (right) of the active CoRe-gel at 600°C in 5% NH_3 at the Re L_{III}-edge compared with references.

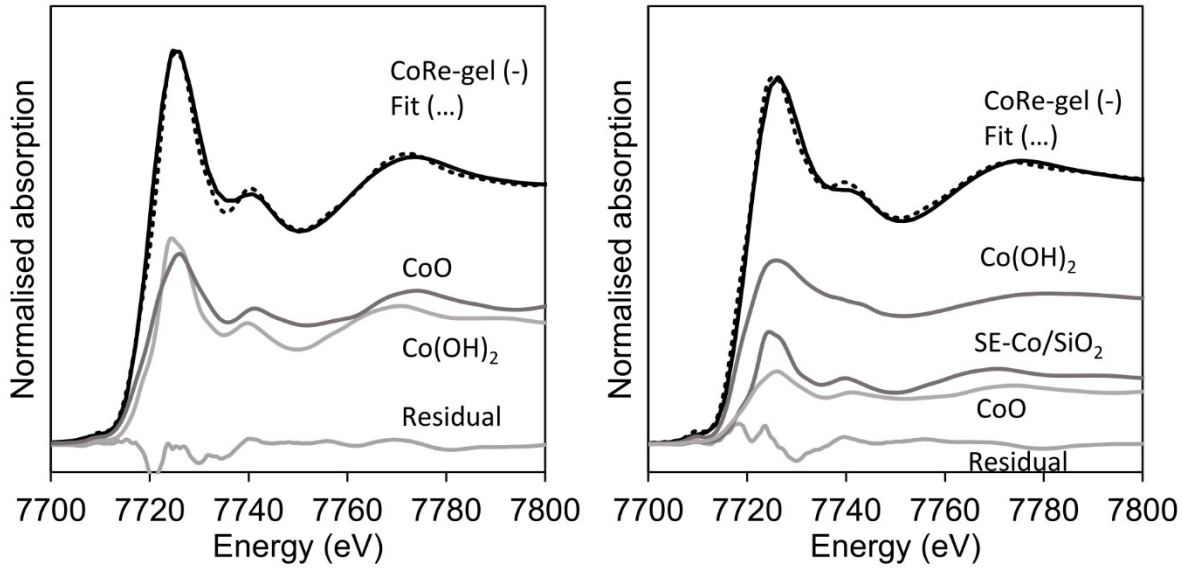

S 12. Linear combination fitting results of the Co-gel (left) and the CoRe-gel (right) with CoO, $Co(OH)_2$ and cobalt in single entities in a silica aerogel.

Table S 3. Linear combination fitting results of the as synthesised Co-gel and the as synthesised CoRe-gel, with CoO, $Co(OH)_2$ and Single Entities (SE)-Co/SiO_2.

Sample	CoO	$Co(OH)_2$	SE-Co/SiO_2	R-factor*
Co-gel	0.55(5)	0.45(5)	0	0.003992
CoReGel	0.24(3)	0.21(5)	0.55(3)	0.00299

*R-factor obtained from the Athena software

Identification of surface groups during annealing of the silica aerogels.

Experimental:

Diffuse Reflectance Infrared Fourier Transform Spectroscopy was performed with a Bruker Vertex 80 with a LN-MCT detector between RT and 450°C and a DTGS detector between from 450-650°C. The sample (14 mg) in a ceramic cup was loaded into a high temperature cell from Pike Technologies and annealed to 450°C for 30 min, consecutively the sample was annealed to 650°C for 1 hour the heating rate was 3°C min^{-1}. The flow of synthetic air was set to 15 ml min^{-1}. Spectra were collected *in-situ* from 800-4000 cm^{-1} every minute.

Results:

DRIFTS was performed on the as-synthesised samples to investigate the thermal stability of the hydrophobic surface of the support. Kristiansen and co-workers[1] investigated the spectral region containing the vibrational modes of the surface groups adsorbed species during annealing copper aerogels to 450°C. They found vibration bands associated with adsorbed water, surface hydroxylic groups, adsorbed ammonia and methyl groups at the aerogel surface. The annealing (S 13) of the CoRe-aerogel shows clear bands at 2963 cm^{-1} and 2906cm^{-1} corresponding to the $\nu_{s\text{-}C\text{-}H}$ and $\nu_{as\text{-}C\text{-}H}$ modes.[1, 2] The surface hydroxyl mode, $\nu_{O\text{-}H,}$ visible for all spectra in the region of 3700-3710 cm^{-1} becomes more apparent during heating due to the removal of adsorbed water as seen by the decrease of intensity in the region of 3100 – 3650 cm^{-1}. Also two small low intensity bands at 3368 cm^{-1} and 3280 cm^{-1} become visible at 100°C and are associated with NH_3 vibrational modes originating from the surface modification.[3] The decrease in the intensity of the $\nu_{s\text{-}C\text{-}H}$ and $\nu_{s\text{-}C\text{-}H}$ starts at 100°C and continues until extinction of the signal after 1 hour at 650°C (S 4).

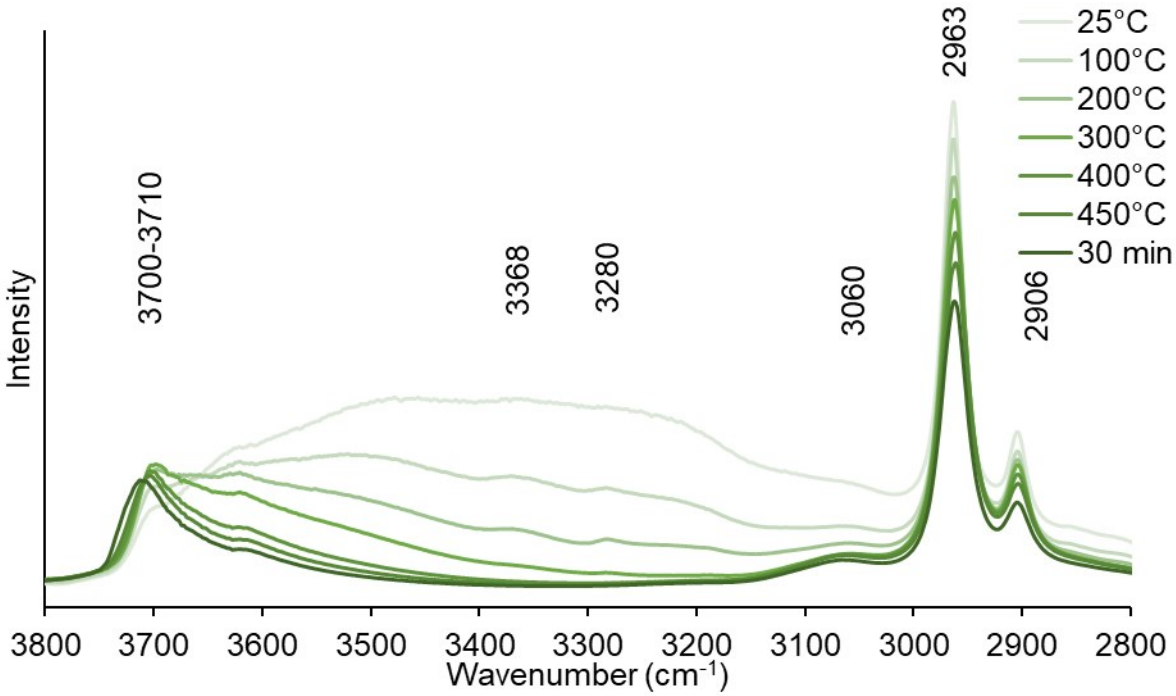

S 13. FT-IR of the *in situ* annealing of the CoRe-gel at selected temperatures.

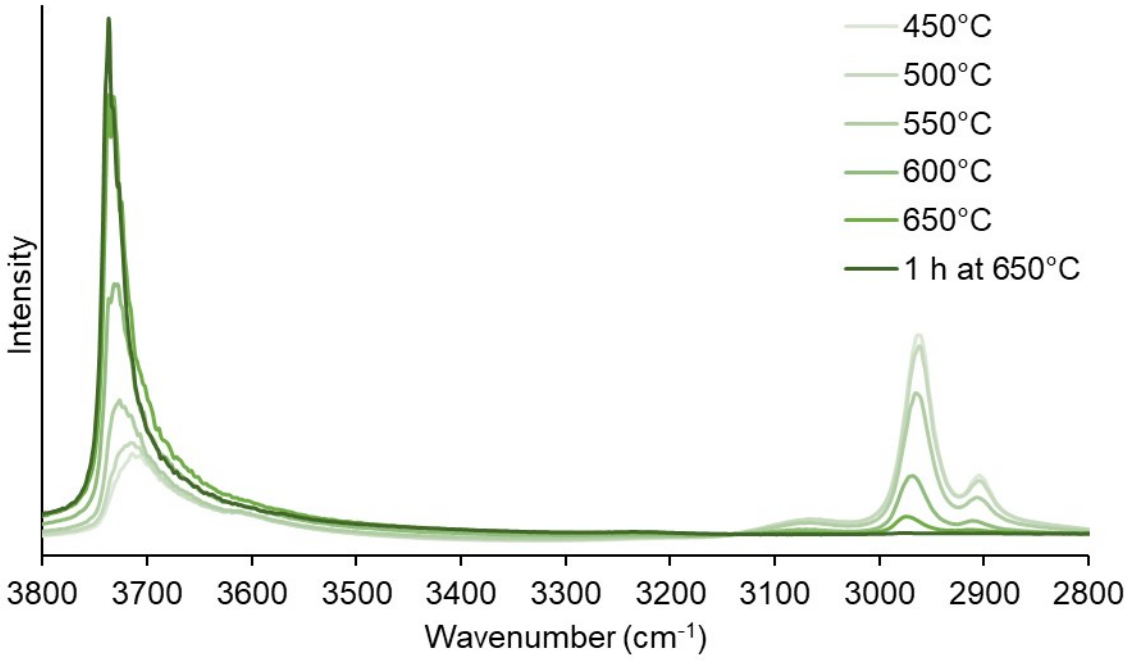

S 14. In situ FT-IR of the calcination process up to 650°C at selected temperatures.

The *in-situ* calcination of the CoRe-gel monitored by FT-IR (S 14) demonstrates that complete loss of -CH_3 vibrational modes is achieved after 60 min at 650°C. The intensity of the surface hydroxyl groups on the aerogel support increases as the hydrophobic surface is burnt off due to oxidation of the methyl groups.

Phase determination during *in-situ* reduction and ammonia decomposition of CoRe-gel.

In-situ powder X-ray diffraction for the as-synthesised CoRe-gel (S 15) show a diffraction pattern consistent with the presence of the NH_4ReO_4 phase (Figure 1 in the main paper). The pre-treated CoRe-gel show reflections resembling reduced unsupported CoRe where reflections were assigned to bimetallic CoRe and monometallic rhenium.[4]

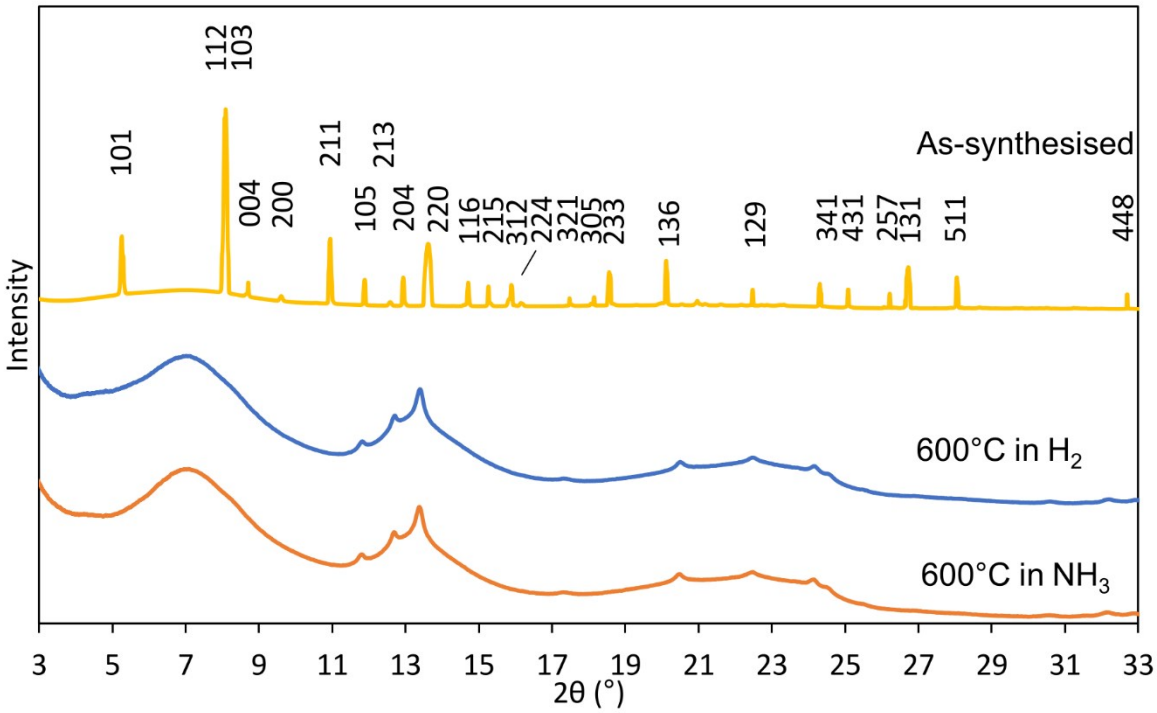

S 15. In-situ XRD (synchrotron wavelength) of the as-synthesised sample, after pre-treatment in H_2 at 600°C and during ammonia decomposition at 600°C.

Table S 4. EXAFS-least squares refinements of the as synthesised, annealed, and pre-treated Co-gel.

Treatment	Shell	N	R (Å)	$2\sigma^2$ (Å^2)	E_F (eV)	R (%)	Δk	AFAC
As synthesised	Co-O	5.1(6)	2.11(1)	0.019(4)	-7.0(7)	36	2-10	0.78
	Co…Co	7(1)	3.143(7)	0.021(4)				
Annealed	Co-O	4.4(3)	2.07(1)	0.022(3)	-8.2(7)	44	2-10	0.78
	Co…Co	5(1)	3.09(2)	0.038(5)				
Pre-treated	Co-O	3.2(5)	2.00(1)	0.019(5)	-7.4(9)	42	2-10	0.66
	Co…Co	3(2)	2.99(3)	0.04(2)				

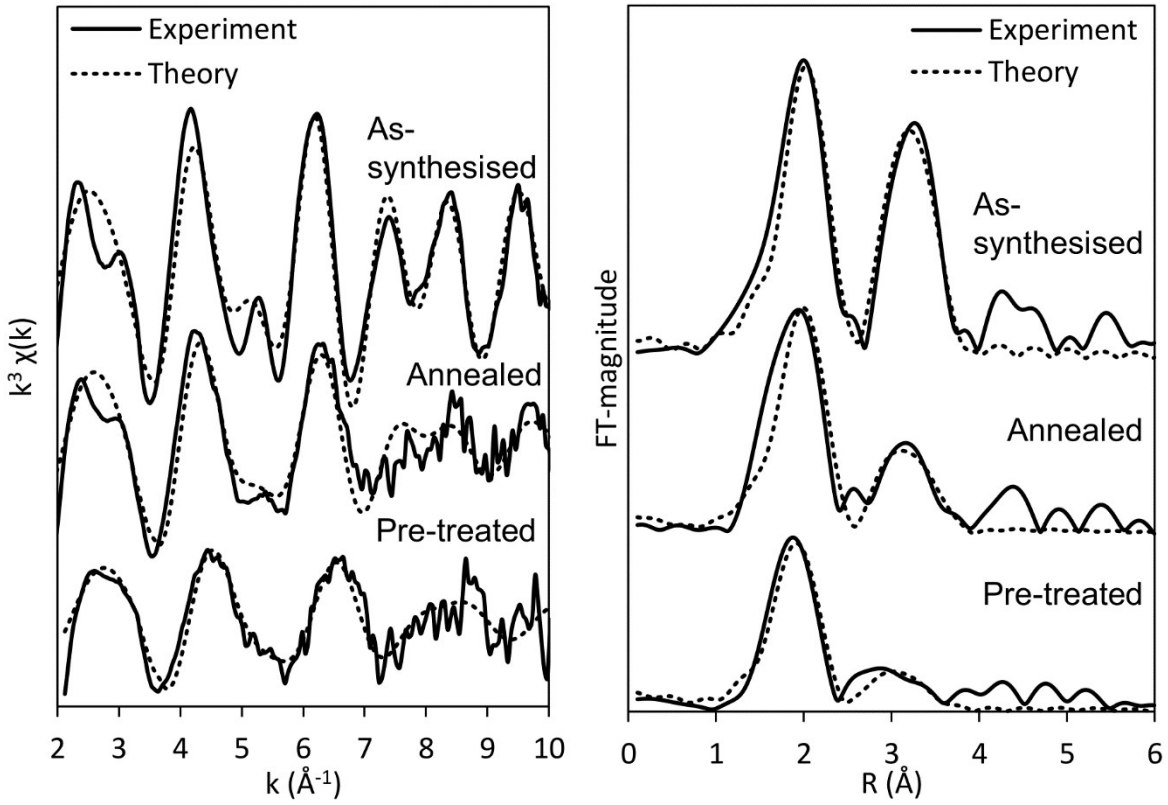

S 16. EXAFS-analysis of the annealed (top) and after pre-treatment (bottom) Co-gel with chi-curves (left) and the FT transformed curves (right) at the Co K-edge.

Table S 5. Results of EXAFS-analysis of the Fourier filtered data of the backscattered metallic contribution in the CoRe-gel at 600°C in 5% NH_3 at the Co K-edge and Re L_{III}-edge.

Shell	N	R (Å)	$2\sigma^2$ (Å^2)	E_F (eV)	R (%)	Δk	AFAC	Real space range (Å)
Co-Co	0.6(1)	2.538(6)	0.012(4)	-21.3(6)	35	2-9	0.79	2.1-3.15
Co-Re	1.3(2)	2.575(5)	0.013(2)	-8.8(6)	25	2-9	0.79	2.1-3.15
Co-Co + Co-Re	Unsuccesfull fit.							
Re-Co	3.9(6)	2.60(1)	0.033(3)	-13(1)	22	3-9.5	0.8	2-3.4
Re-Re	9(1)	2.658(9)	0.033(3)	-5(1)	31	3-9.5	0.8	2-3.4
Re-Co + Re-Re	2.7 (5) 2.5(9)	2.570(5) 2.72(2)	0.031(4) 0.029(7)	-9.9(9)	19	3-9.5	0.8	2-3.4

Multivariate curve resolution with alternating least square algorithm – description and application

Multivariate curve resolution with alternating least square algorithm (MCR-ALS)[5-8] was used to analyze the *in situ* time-resolved (TR) XANES data for the CoRe-gel during the pre-treatment step in 75% H_2.. MCR is well-known for its capabilities of blindly separating (i.e. no references needed) TR spectra into a set of meaningful component spectra and their corresponding concentration profiles. For the assessment of the minimum number of principal components that describe the system i.e. rank analysis, a built-in method based on the singular value decomposition (SVD) was used, and this was combined with a comprehensive principal component analysis (PCA, *vide infra*) study.[9] The SVD results display the calculated eigenvalues of the data versus the component number (the so-called scree plot), which allows understanding how much variance each component can explain. A break in the slope of such a plot is generally associated to the minimum number of components able to simulate the initial mixture. On the other hand, PCA has been used as an alternative and complementary tool to reduce the dimensionality of the *in situ* XANES to a minimum no. of representative components.

The MCR-ALS graphical user interface (GUI) for Matlab® used in the present manuscript (http://www.mcrals.info/) was applied on the normalised XANES at theCo K-edge and Re L_{III}-edge (i.e. Co: 7700-7770 eV and Re: 10520-10570 eV). Positive constraints for both concentration and spectra profiles and closure constraints for the concentration (i.e. no mass transfer; constant concentration of the absorber, Co/Re, throughout the TR experiment) were utilised. Mathematically, the MCR model [5-8] is described by the equation $\mathbf{D} = \mathbf{CS^T} + \mathbf{E}$, with **D** being the initial mixture (a matrix made-up from all the spectra collected), and **C** and **S** (T: transpose matrix) are the extracted concentration and spectra profiles, respectively. **E** is the residuals matrix and it is close to the experimental error when convergence is achieved. Furthermore, a set of fitting parameters[5, 6, 10] are used to judge the consistency of the MCR-ALS solutions for both cobalt and rhenium. The explained variance (equation **1**), the lack of fit parameter (equation **2**), and the standard deviation of residuals (equation **3**) with respect to the experimental data evaluate to what extent the MCR model reflects the experimental results.

$$R^2 = 100\sqrt{\frac{\sum_{i,j} d_{ij}^2 - \sum_{i,j} e_{ij}^2}{\sum_{i,j} d_{ij}^2}} \qquad [\mathbf{1}]$$

$$Lack\ of\ Fit\ (\%) = 100\sqrt{\frac{\sum_{i,j} e_{ij}^2}{\sum_{i,j} d_{ij}^2}} \qquad [\mathbf{2}]$$

$$\sigma = \sqrt{\frac{\Sigma_{i,j} e_{ij}^2}{n_{rows} n_{columns}}} \qquad [\mathbf{3}]$$

In the equations **1**, **2**, and **3** d_{ij} is an element of the experimental data matrix, e_{ij} is the residual value (i.e. initial data – simulated data) and n_{rows} and $n_{columns}$ are the number of rows and columns of the initial D matrix.

Table S 6. MCR-ALS fitting results, i.e. goodness of fit parameters, for the Co K-edge *in situ* XANES by using a 3-component system. The convergence is achieved, and the plots are optimum at the iteration no. 14.

Fitting parameter	Result
Standard deviation of residuals vs. experimental data	0.002188
Fitting error (lack of fit, LOF) in % (PCA)	0.16551
Fitting error (lack of fit, LOF) in % (experimental)	0.25494
Percent of variance explained	99.9994

Table S 7. MCR-ALS fitting results, i.e. goodness of fit parameters, for the Re L_{III}-edge *in situ* XANES by using a 3-component system. The convergence is achieved, and the plots are optimum at the iteration no. 21.

Fitting parameter	Result
Standard deviation of residuals vs. experimental data	0.0049228
Fitting error (lack of fit, LOF) in % (PCA)	0.34977
Fitting error (lack of fit, LOF) in % (experimental)	0.37965
Percent of variance explained	99.9986

Principal component analysis (PCA) for the identification of the minimum number of components

A critical step of the MCR-ALS routine is represented by the assessment of the number of components to be used in the run and able to simulate the initial data with minimum error. We employed a combined approach involving a preliminary PCA carried out by using PrestoPronto[11] software (Python based freeware with a GUI), and we further combined this with the MCR-ALS own rank analysis method based on the scree plot analysis (i.e. SVD method). The results for both Co (**S 17** a-d) and Re (**S 18a-d**) edges in parallel with the aim of justifying the choice of a 3-component system during the MCR-ALS runs.

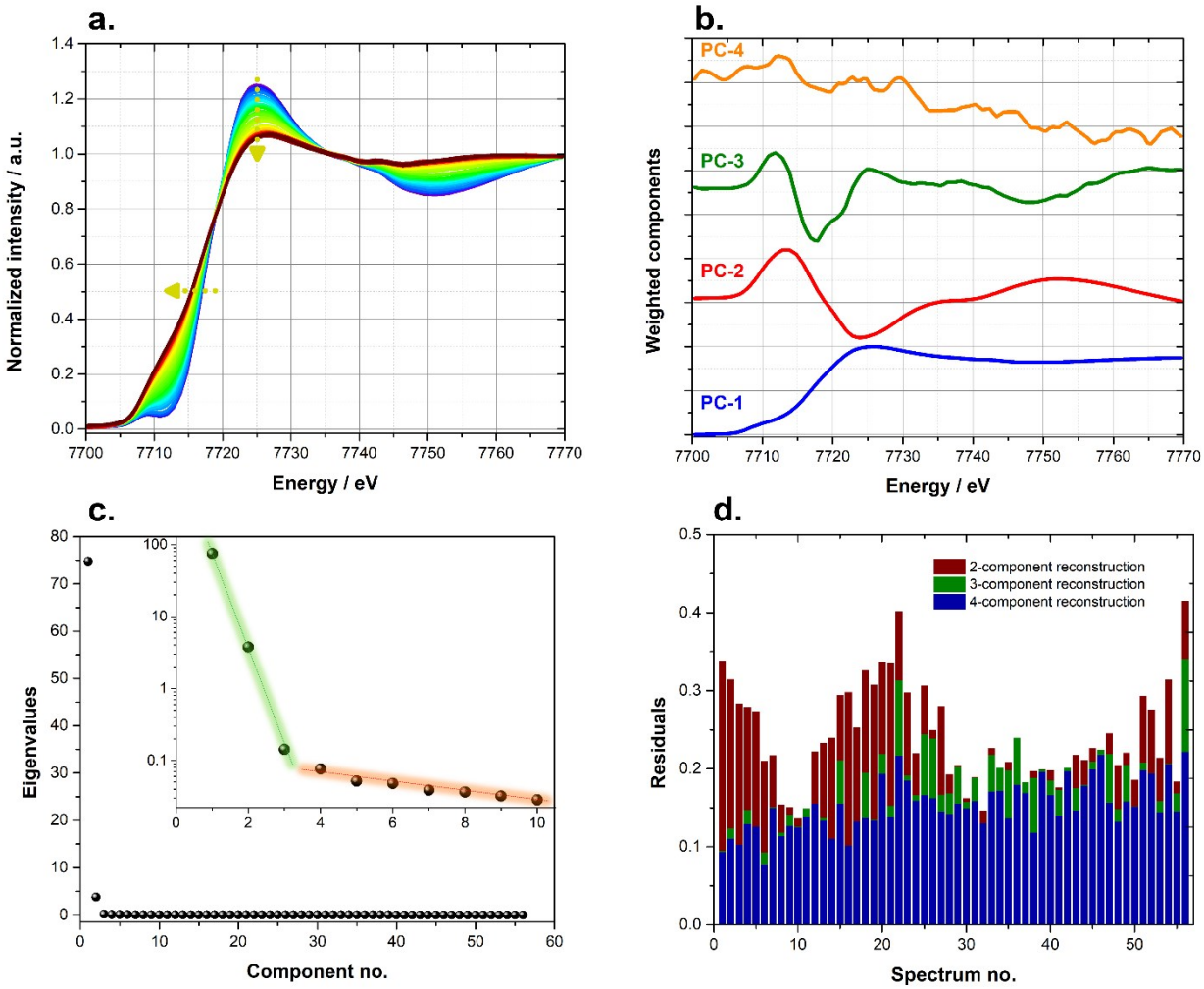

S 17. Results of the PCA analysis at the Co K-edge *in situr* XANES a) time-resolved data with the two arrows pointing at the changes occurring during the pre-treatment in 75% H_2.. b) first 4 principal components as extracted with the PrestoPronto software. The components are normalized for clarity. c) Scree plot representation of the eigenvalues using a linear scale and the inset, in logarithmic scale, displaying the first 10 eigenvalues and the "knee" formation. Results from the SVD rank analysis integrated in the MCR-ALS algorithm. d) Residuals obtained from the time-resolved data-set reconstruction by using a mixture of 2 (dark-red), 3 (green), and 4 (blue) principal components, respectively. Results from PCA reconstruction using PrestoPronto.

First of all, by having a look over Co (**S** 17 **a**) and Re (**S 18 a**) *in situ* XANES acquired during the pre-treatment in 75% H_2, we can clearly identify a reductive behaviour towards their metallic state for both Co and Re i.e. this comes from a drastic reduction of the white-line intensity and the shift of the absorption edge (with ca. 3-4 eV) towards lower energies. The goal now becomes to detect if this transition from a more oxidized to a more metallic state of Co/Re happens *via* a (one or more) transition state(s) or not, and how those states look like in terms of chemical environment, oxidation states, etc (see the MCR-ALS results in the manuscript).

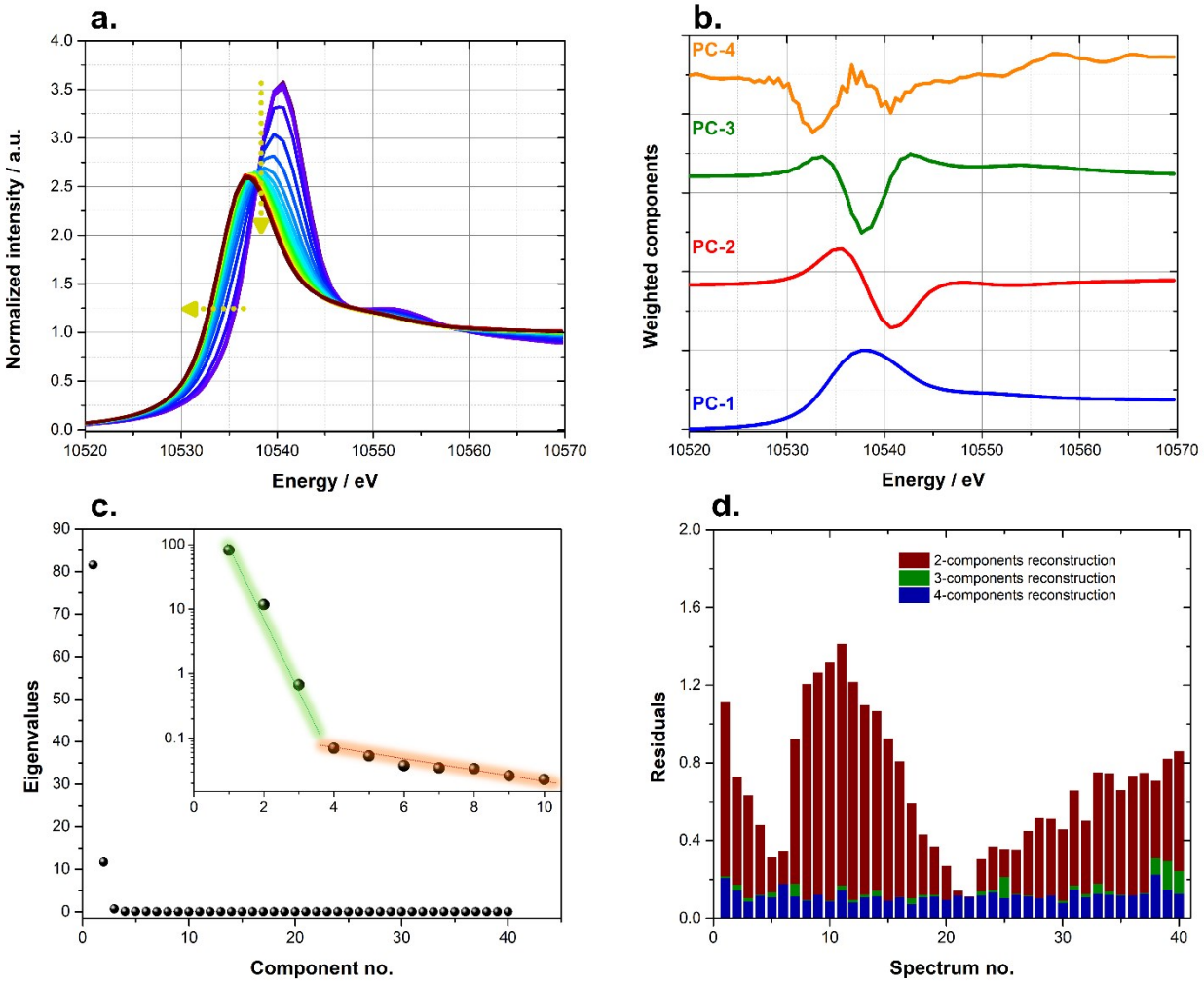

S 18. Results of the PCA analysis at the Re L_{III}-edge *in situ* XANES of the CoRe-gel during pre-treatment.a) time-resolved data with the two arrows pointing at the changes occurring during the pre-treatment in 75%H_2 pre-treatment. b) first 4 principal components as extracted with the PrestoPronto software. The components are normalized for clarity. c) Scree plot representation of the eigenvalues using a linear scale and the inset, in logarithmic scale, displaying the first 10 eigenvalues and the "knee" formation. Results from the SVD rank analysis integrated in the MCR-ALS algorithm. d) Residuals obtained from the time-resolved data-set reconstruction by using a mixture of 2 (dark-red), 3 (green), and 4 (blue) principal components, respectively. Results from PCA reconstruction using PrestoPronto.

For this purpose, **S** 17**b** and **S 18b** display the first 4 PC extracted from PrestoPronto and normalized for a clearer interpretation. On the one hand, the Co case clearly shows how the first 3 PC (blue, red, green) account for all the changes in the XANES region of the spectra, whereas the 4th component (in orange) is constituted mostly from noise and does not show any specific XANES features. On the other hand, the Re case has 3 major constituents (blue, red, and green) that – likely – cover for all the important changes in the pre-edge, absorption edge and white-line position; the 4th component, although envisioning some very minor features in the region of absorption edge and white line, seems to be dominated by high-frequency noise and it was discarded following the subsequent SVD analysis and PC reconstruction methodology (*vide infra*). The scree plots presented in **S** 17**c** and **S 18c** show an eigenvalue representation [10, 12, 13] (i.e. a measure of for how much variance every component in the system can explain) as a function of the component number. The logarithmic scale representation in the inset (for both Co and Re cases) makes it relatively easy to differentiate the presence of a 3-component system in both Co and Re by looking for the famous break (or "knee") in the plot (the components after the 3rd one have eigenvalues that align in a more linear fashion and with much smaller values than the first 3). As a last complement to this analysis, a data reconstruction protocol was performed for the original data with 2, 3, and 4 PC, respectively. The results of these reconstructions are shown in the **S** 17**d** and **S 18d** for both cobalt and rhenium. While for the Co case, the residuals improve significantly with the introduction of a 3rd component (especially in the first half of the *in situ* measurement; in green) as compared to a 2-component reconstruction (in dark-red), for the Re case the improvement is even more important (6-fold better) when a 3-component reconstruction has been performed *versus* a 2-component one (same color coding). In both cases, the introduction of a 4th component in the simulations (in blue color) does not justify the choice for a 4-component system for the MCR-ALS (in either case) as no significant decrease in the residuals has been further detected. Therefore, we can conclude that by applying this combined PCA/SVD approach, choosing a 3-component system to describe both the Co and Re cases is the correct choice for the investigated catalysts; lastly, the as-extracted MCR-ALS spectra and concentration profiles have clear physico-chemical fundaments and meaning as demonstrated in the manuscript.

References

1. T. Kristiansen, K. Mathisen, M. A. Einarsrud, M. Bjorgen and D. G. Nicholson, *Journal of Physical Chemistry C*, 2011, **115**, 19260-19268.
2. R. Al-Oweini and H. El-Rassy, *Journal of Molecular Structure*, 2009, **919**, 140-145.
3. F. Poignant, J. Saussey, J.-C. Lavalley and G. Mabilon, *J. Chem. Soc., Chem. Commun.*, 1995, 89-90.
4. K. Mathisen, K. G. Kirste, J. S. J. Hargreaves, S. Laassiri, K. McAulay, A. R. McFarlane and N. A. Spencer, *Top Catal*, 2018, **61**, 225-239.
5. J. Jaumot, R. Gargallo, A. de Juan and R. Tauler, *Chemometrics and Intelligent Laboratory Systems*, 2005, **76**, 101-110.
6. J. Jaumot, A. de Juan and R. Tauler, *Chemometrics and Intelligent Laboratory Systems*, 2015, **140**, 1-12.
7. C. Ruckebusch and L. Blanchet, *Anal Chim Acta*, 2013, **765**, 28-36.
8. A. Voronov, A. Urakawa, W. van Beek, N. E. Tsakoumis, H. Emerich and M. Ronning, *Anal Chim Acta*, 2014, **840**, 20-27.
9. S. R. Wasserman, *Le Journal de Physique IV*, 1997, **7**, C2-203-C202-205.
10. M. Staniuk, O. Hirsch, N. Kränzlin, R. Böhlen, W. van Beek, P. M. Abdala and D. Koziej, *Chemistry of Materials*, 2014, **26**, 2086-2094.
11. S. J. A. Figueroa and C. Prestipino, *Journal of Physics: Conference Series*, 2016, **712**, 012012.
12. A. Martini, E. Borfecchia, K. A. Lomachenko, I. A. Pankin, C. Negri, G. Berlier, P. Beato, H. Falsig, S. Bordiga and C. Lamberti, *Chemical Science*, 2017, **8**, 6836-6851.
13. A. Tsoukalou, P. M. Abdala, D. Stoian, X. Huang, M.-G. Willinger, A. Fedorov and C. R. Müller, *Journal of the American Chemical Society*, 2019, **141**, 13497-13505.